Magnetic properties of melt-quenched amorphous Fe$_2$(B$_{1-y}$Zr$_y$) $(0 \leqslant y \leqslant 0.55)$

LETTER TO THE EDITOR

Magnetic properties of melt-quenched amorphous Fe$_2$(B$_{1-y}$Zr$_y$) (0 $\leqslant$ y $\leqslant$ 0.55)

D Kaptás†, T Kemény†, J Balogh†, L Bujdosó†, L F Kiss†, T Pusztai†‡ and I Vincze†‡

† Research Institute for Solid State Physics and Optics, H-1525 Budapest, POB 49, Hungary
‡ Department of Solid State Physics, Eötvös University, Budapest, Hungary

Abstract. Amorphous Fe$_2$(B$_{1-y}$Zr$_y$) alloys, which are important as the residual amorphous matrices in nanocrystalline Fe–Zr–B–Cu systems, were prepared by rapid quenching from the melt for 0 $\leqslant$ y $\leqslant$ 0.55. The iron magnetic moment determined by ^{57}Fe Mössbauer spectroscopy and magnetic measurements shows an unexpected initial increase when Zr is substituted for B. This behaviour, together with the uncommon crystallization sequence, is attributed to the highly attractive B–Zr interaction.

Nanocrystalline Fe–Zr–B–Cu alloys [1] form a new class of soft magnetic composite materials with high initial magnetic permeability and low coercivity. They consist of nanosize ferromagnetic granules embedded in an amorphous matrix. These nanocrystalline alloys are prepared by partial crystallization of amorphous ribbons, which results in crystalline bcc precipitates a few nanometres in size in a residual amorphous matrix whose characteristic size is also in the nanometre range. Despite an intensive research effort, the magnetic properties and the chemical composition of this rather inhomogeneous residual amorphous phase are not well known. Recent Mössbauer evaluation [2] of the amount of precipitated Fe-based solid solution (with a total impurity content estimated [2] to be less than 4 at.% on the basis of the Mössbauer data) indicates that the Fe content of the remaining amorphous phase is significantly decreased and approaches 67 at.% Fe. The Fe–B–Zr amorphous alloys in the 74–90 at.% Fe content range have been investigated [3], but the properties are unknown for compositions with lower Fe contents. The aim of the present article is the preparation and the investigation of these formerly not studied amorphous Fe$_2$(B, Zr) alloys. It will be shown that both the crystallization and the magnetic properties depend on the Zr content in ways which are qualitatively different to those that were seen for the composition range studied before. The results will be compared to the well-known properties of the two related stoichiometric crystalline compounds Fe$_2$B and Fe$_2$Zr.

Melt-quenched Fe$_2$(B$_{1-y}$Zr$_y$) ribbons are amorphous in the 0 $\leqslant$ y $\leqslant$ 0.55 composition range when they are melt spun with an effective heat contact (i.e. in vacuum) and are thinner than 12 μm. The amorphicity of the alloys was checked by Mössbauer spectroscopy and x-ray diffraction. Our attempts to prepare amorphous alloys by melt quenching above y = 0.55 were unsuccessful; the samples had crystalline traces. The study of the crystallization behaviour of the ribbons provided a further control for the samples.

The Mössbauer measurements were carried out using a conventional constant-acceleration spectrometer with a 50 mCi ^{57}Co**Rh** source at room temperature. An APD closed-cycle

cryostat and a home-made vacuum furnace were used for the low- and high-temperature measurements. The saturation magnetic moments of the alloys were determined from the magnetization measured at 12 K in the 0–5 T external magnetic field range using an MPMS-5S SQUID magnetometer. The high-field susceptibility of the alloys is rather small and increases with the Zr content: it is 0.9×10^{-3} μ_B T^{-1}/(Fe atom) for the $y = 0$ alloy, while it attains 3.7×10^{-3} μ_B T^{-1}/(Fe atom) for the $y = 0.5$ composition.

The thermal behaviour was investigated by a SETARAM DSC92 calorimeter in the 600–1200 K temperature range and by a Perkin–Elmer DSC-2 instrument which is restricted to working below 1000 K but attains a higher sensitivity. 5–20 K min^{-1} heating rates were applied. The usual calibration and evaluation procedures were applied. Due to the smaller sensitivity of the SETARAM 92 calorimeter, the measurements show an enhanced noise level and are presented here after smoothing by the standard averaging method. The structure of the crystalline phases was determined by x-ray diffraction measurements performed on a Philips Xpert diffractometer.
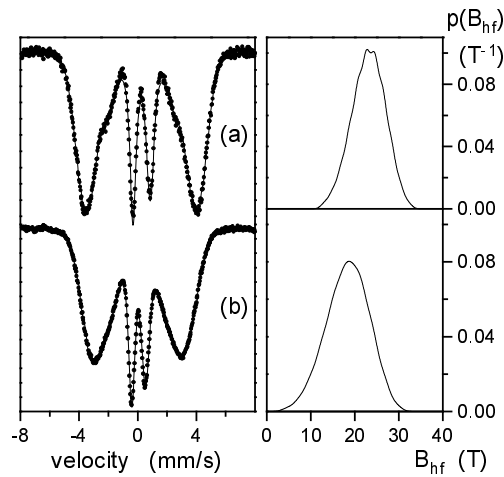

Figure 1. Mössbauer spectra and the hyperfine field distributions for amorphous Fe_2B (a) and $Fe_2B_{0.5}Zr_{0.5}$ (b) measured at 12 K.

Typical Mössbauer spectra of the amorphous samples measured at 12 K are shown in figures 1(a) and 1(b), respectively. The broad lines reflect a distribution of the hyperfine parameters; the shape of the hyperfine field distribution, $p(B_{hf})$, was fitted by a double-binomial distribution [4]. Linear correlation between the hyperfine field, the isomer shift and the quadrupole splitting was assumed. The linewidths of the individual six-line patterns, together with the intensity of lines 2–5, I_{2-5}, were determined by least-squares fitting of the spectra. The values of I_{2-5} obtained at low temperatures were significantly smaller than the room temperature ones, which is a consequence of the positive magnetostriction [5] of the samples, which are under external stress due to the Scotch tape® applied in the mounting. This reflects a magnetic anisotropy perpendicular to the surface of the ribbons. The shapes of the $p(B_{hf})$ distributions are quite structureless; slight broadening is observed for increasing Zr content.

The complex process of crystallization is illustrated in figure 2(a) for the $y = 0, 0.125$ and 0.25 samples. As is illustrated in figure 2(b), the starting temperature of crystallization increases significantly up to $y = 0.5$. It is usual for a refractory addition to increase the crystallization temperature by hindering atomic diffusion through increased atomic binding. The significant initial decrease for the heat of crystallization of the first stage (figure 2(c)) is remarkable. It is connected to the change of crystallization product from Fe_2B to Fe_3B as
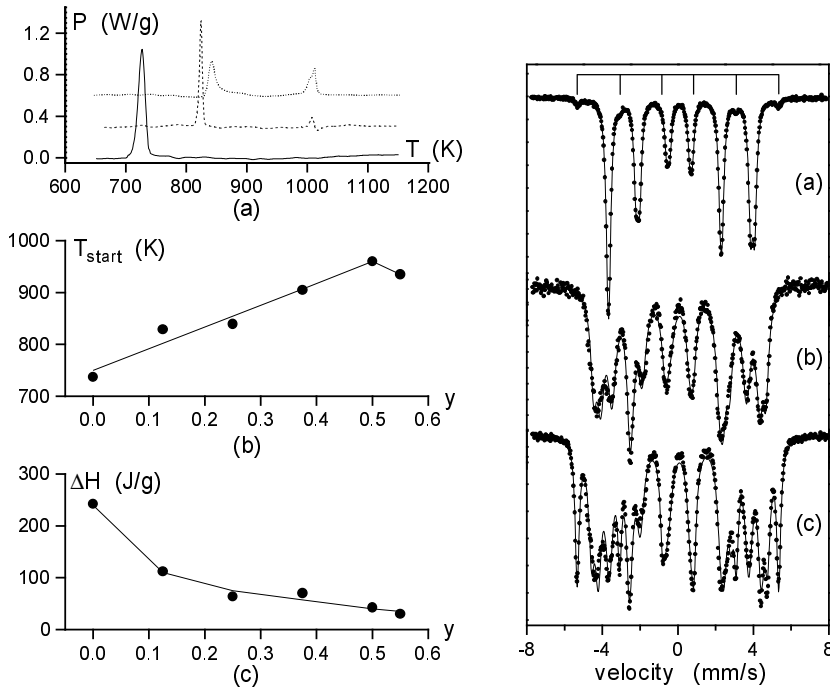
Figure 2. (a) DSC transformations of the $y = 0$ (solid curve), $y = 0.125$ (shifted by 0.3 W g^{-1}; dashed curve) and $y = 0.25$ alloys (shifted by 0.6 W g^{-1}; dotted curve) measured with 5 K min^{-1} heating rates. (b) The starting temperature of the transformation. (c) The heat of transformation for the first stage (evaluated from 20 K min^{-1} Perkin–Elmer DSC2 measurements).
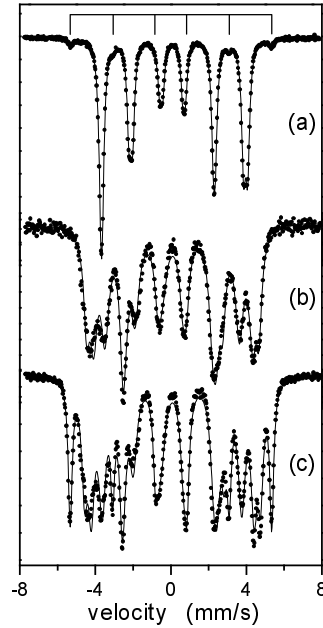
Figure 3. Room temperature Mössbauer spectra of crystallized Fe_2B (a) and $Fe_2B_{0.875}Zr_{0.125}$ taken after the first (b) and the second step (c) of the transformation process. The position of the six-line pattern of α-Fe is shown. The rest of the spectra correspond to crystalline Fe_2B (a) and Fe_3B ((b) and (c)).

will be discussed below. The transformation energy of the $Fe_3B \rightarrow Fe_2B + \alpha$-Fe reaction was found [6] to be 1.5 kJ mol^{-1} (33.5 J g^{-1} for Fe_3B). Also, the significantly decreased heat of crystallization hints that an amorphous fraction remained after the process, which transforms further in the second heat evolution stage.

The amorphous Fe_2B crystallized in a single step to the well-known crystalline Fe_2B compound with C16 structure [7]. The room temperature Mössbauer spectrum in figure 3(a) reveals only a small amount of α-Fe in addition to the Fe_2B contribution (corresponding to about 0.8 at.% excess Fe) which limits the deviation between the real and nominal compositions of the samples to the 1 at.% range. The crystallization of the $Fe_2B_{0.875}Zr_{0.125}$ sample—though much more complicated—supports this estimate. After the first step of the transformation, crystalline Fe_3B is the only component [8] found in both the Mössbauer spectrum (figure 3(b)) and the x-ray diffractogram. The absence of a measurable amount of Zr in the Fe-containing phase implies that the remaining material should be an almost Fe-free B–Zr alloy; its average composition is estimated as $B_{60}Zr_{40}$, and its atomic fraction is about 11%. The lack of Zr-containing crystalline phase in the x-ray pattern indicates that this material may have a broad composition distribution and has a very small grain size or might even be amorphous.

On further annealing (after the second stage of the transformation in the DSC), α-Fe surprisingly appears beside the Fe_3B component (figure 3(c)). From their fraction in the Mössbauer spectra, an apparent 80 at.% average Fe content is estimated for the Fe-containing

phases. The B:Zr ratio of the phase remaining after this transformation is estimated from the amount of α-Fe and Fe_3B using the original composition and it indicates further B enrichment towards the ZrB_2 stable compound. While the thermal process is finished in the temperature range of this study (figure 2(a)), a sufficiently large grain size of the expected structure is not yet evolved, as x-ray diffraction did not detect the stable ZrB_2 structure. The very high melting point [9] (3200 °C) of this compound hints at a considerable binding energy, i.e. a significant driving force for its formation. The appearance of the significant amount of α-Fe observed in both Mössbauer spectroscopy and x-ray diffraction means that, in the second stage of transformation, Fe_3B reacts with the previously discussed B–Zr phase to initiate the (probably sluggish) formation of a phase with the highest stability known, B_2Zr. The presence of this phase is assumed on an indirect basis, as there is no direct x-ray evidence for its formation. The unusual sequence of crystallization indicates that the processes are dominantly influenced by the Zr–B pair energy, which has a much more negative value than the Fe–B and Fe–Zr pair energies. Similar reaction is assumed in the crystallization of the amorphous samples with larger Zr content, but the crystal structures in the ternary Fe–Zr–B phase diagram are not known. In this context it is remarkable that the Fe_3B structure is observed at about 1100 K while in binary alloys its existence is limited to below 900 K even under high-pressure conditions [10].

Figure 4 summarizes the composition dependence of the Mössbauer parameters evaluated (and the saturation moment) for the amorphous alloys. The isomer shift (figure 4(a)) follows
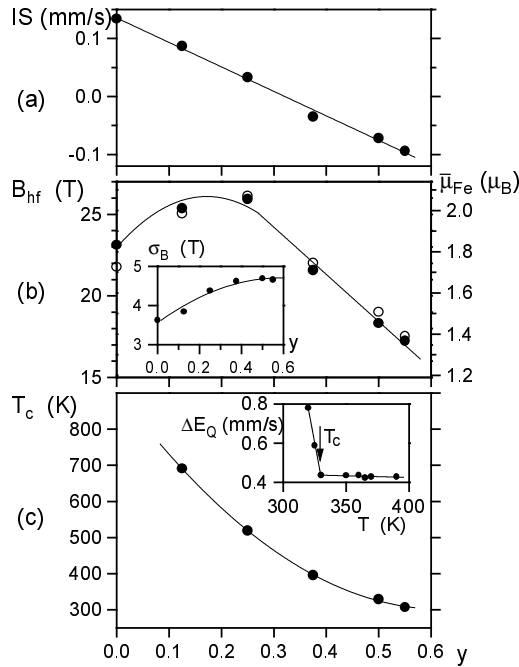

Figure 4. The composition dependences of the average Fe isomer shift, IS, at room temperature with respect to that of α-Fe (a), of the average Fe hyperfine field, B_{hf} (left-hand scale, filled circles), and iron saturation moment, $\bar{\mu}_{Fe}$ (right-hand scale, empty circles), at 12 K (b) and of the Curie temperature (c). The inset in (b) shows the composition dependence of the standard width of the hyperfine field distribution σ_B. The Curie temperatures are determined from the temperature dependence of the average quadrupole splitting ΔE_Q as shown for $Fe_2B_{0.5}Zr_{0.5}$ in the inset of (c).

the trend set by the crystalline compounds Fe_2B and Fe_2Zr. Fe_2B has a C16 body-centred tetragonal crystal structure, where the Fe atoms are surrounded with four B nearest neighbours and eleven Fe nearest neighbours; its isomer shift is 0.12 mm s^{-1} with respect to that of α-Fe at room temperature [7]. In the C15 Laves phase crystal structure of Fe_2Zr, the single Fe sites have six Zr and six Fe nearest neighbours; the Fe isomer shift is -0.18 mm s^{-1} [11]. The observed smooth composition dependence for the amorphous $Fe_2(B_{1-y}Zr_y)$ alloys indicates that the isomer shift, i.e. the charge density at the Fe sites, is insensitive to the actual topological position of the B and Zr nearest neighbours, probably because of the averaging effect of the large coordination number; thus it measures only the average number of B and Zr neighbours.

On the other hand, the composition dependences of the Fe hyperfine field and the low-temperature saturation magnetic moment are both quite unusual (figure 4(b)): they start to increase with increasing Zr content, then display a maximum followed by the expected decrease at higher Zr compositions. In the crystalline compounds the saturation values of the iron magnetic moment and hyperfine field are 1.91 μ_B and 24.8 T for Fe_2B and 1.45 μ_B and 21.9 T for Fe_2Zr [7, 11]. Crystalline magnetic anisotropy splits the hyperfine field values by less than 1 T in both systems. The Fe magnetic moment was found to be proportional to the Fe hyperfine fields: for the crystalline Fe–B compounds the proportionality constant is about 13 T μ_B^{-1} [12], while for the compounds of Fe with early transition metals, 14.5 T μ_B^{-1} is reported [13]. In the present case, hyperfine fields and magnetic moments are found to be proportional, as is shown in figure 4(b), where the proportionality constant corresponds well to the 13 T μ_B^{-1} characteristic for the known Fe–B compounds.

The weak composition dependence of the standard width of the Fe hyperfine field distributions, σ_B, shown in the inset of figure 4(b), is well explained by the effect of fluctuating B and Zr environments; a simple estimate based on the crystalline values would indicate less than 1 T extra broadening at $y = 0.5$.

The Curie temperature of these alloys was determined from the Mössbauer measurements as shown in the inset of figure 4(c): the apparent average quadrupole splitting, ΔE_Q, as determined from a two-line fit in the paramagnetic state quickly increases with decreasing temperature in the magnetic state. Sharp transitions were observed for all alloys investigated; the accuracy for T_c is about ± 1 °C. The Curie temperature decreases monotonically with increasing Zr content though the rate of the decrease is diminished around $y = 0.5$.

Literature data are available for the magnetic properties of Fe–Zr–B amorphous alloys in the 10–74 at.% Fe composition range. From the published ternary plots [3] it is evident that the room temperature saturation magnetization decreases monotonically with increasing Zr content for both the $Fe_{80}Zr_xB_{20-x}$ and the $Fe_{75}Zr_xB_{25-x}$ series. Very similar trends have also been published [14] for many early transition metals in the case of $Fe_{80}TM_xB_{20-x}$ alloys (TM = Cr, V, Nb, Mo, Ta, W). Systematic composition dependences of the low-temperature saturation moments for the constant-Fe-content ternary systems are not available. The data of Zhan *et al* [15] indicate an approximate 10–20% decrease for the low-temperature saturation moment of the alloys in the $x = 4$–6 range for the whole series of early transition metals. In view of these literature results, the observed increase in the average Fe hyperfine field, B_{hf}, and in the low-temperature saturation magnetic moment, $\bar{\mu}_{Fe}$, of the amorphous $Fe_2(B_{1-y}Zr_y)$ alloys investigated here is quite unexpected. The increase which is observed only in the case of high-B-content alloys might be connected to the highly negative B–Zr pair energy. This strong interaction hints at a low B–Zr distance, which in turn might increase the Fe atomic volume contributing to the observed increase of the Fe magnetic moment.

It was shown in the present report that both the crystallization and the magnetic properties of amorphous $Fe_2(B_{1-y}Zr_y)$ alloys differ qualitatively from those reported previously for more Fe-rich alloys. In the high-B-content amorphous systems, the B-rich environments attract

Zr due to the highly negative B–Zr bonding energy. Zr-edge EXAFS measurements might be very informative as regards tracing both chemical short-range order and volume effects. Similar effects are also expected for other early-transition-metal substitutions and in the case of nanocrystalline Fe–Zr–B–Cu soft magnets. Two observations are now mentioned in this respect.

The first observation concerns the composition of the Fe-rich bcc nanocrystals. In equilibrium, both Zr and B are insoluble in bcc Fe. Increased solubility (up to about 4%) of these elements in the bcc nanocrystals was deduced from the Curie temperatures decreasing with increasing B content [2, 16]. This may be explained by the enhanced number of Zr–B pairs, due to their strong attraction and size differences.

The second observation is an unexpected increase in the Curie temperature of the residual amorphous matrix with increasing relative Zr content [2, 16] which is opposite to the general trends for the binary amorphous Fe–Zr alloys. Increased atomic volume of Fe due to Zr and B short-range ordering may explain this observation.

The amorphous $Fe_2(B_{1-y}Zr_y)$ alloys investigated are bulk (micrometre-sized) counterparts of the nanosize residual amorphous phase, the connecting tissue between the bcc precipitates in the nanocrystalline Fe–Zr–B–Cu alloys. This is inferred both from the average Fe content of the residual amorphous phase as deduced from the Mössbauer evaluation of the nanocrystallized bcc fraction and from the isomer shift of the residual amorphous phase. Obtaining the composition dependence of the bulk magnetic properties established in the present work is essential if one is to identify size effects in the residual amorphous phase of the nanocrystals.

References

[1] Suzuki K, Makino A, Inoue A and Masumoto T 1991 *J. Appl. Phys.* **70** 6232
[2] Vincze I, Kemény T, Kaptás D, Kiss L F and Balogh J 1998 *Hyperfine Interact.* **113** 123
      Kemény T, Balogh J, Farkas I, Kaptás D, Kiss L F, Pusztai T, Tóth L and Vincze I 1998 *J. Phys.: Condens. Matter* **10** L221
[3] Ohnuma S, Nosé M, Shirakawa K and Masumoto T 1981 *Sci. Rep. RITU* A **29** 254
      Kobayashi H, Onodera H and Yamamoto H 1986 *J. Phys. Soc. Japan* **55** 331
[4] Vincze I 1982 *Nucl. Instrum. Methods* **199** 247
[5] van Diepen A M and den Broeder F J A 1977 *J. Appl. Phys.* **48** 3165
[6] Battezati L, Antonione C and Baricco M 1997 *J. Alloys Compounds* **247** 164
[7] Weisman I D, Swartzendruber L J and Bennett L H 1969 *Phys. Rev.* **177** 465
[8] Chien C L, Musser D, Gyorgy E M, Sherwood R C, Chen H S, Luborsky F E and Walter J L 1979 *Phys. Rev.* B **20** 283
[9] Massalski T B 1986 *Binary Alloy Phase Diagrams* (Metals Park, OH: American Society for Metals)
[10] Yao B, Liu L, Chen W J, Ding B Z and Su W H 1998 *J. Phys. D: Appl. Phys.* **31** 790
[11] Wertheim G K, Jaccarino V and Wernick J 1964 *Phys. Rev.* **135** A151
[12] van der Woude F and Vincze I 1980 *J. Physique Coll.* **41** C1 151
[13] Gubbens P, van Apeldorn J, van der Kraan A and Buschow K H J 1974 *J. Phys. F: Met. Phys.* **4** 921
[14] Hayashi K, Ishikawa W, Hayakawa M, Ochiai Y, Matsuda M and Aso K 1985 *IEEE Transl. J. Magn. Japan* **1** 203
      (Data also published in *Phys. Data Amorph. Met.* 1991 A, B (31-1, 2) Fachinformationszentrum Karlsruhe ISSN 0344-8401)
[15] Zhan W-S, Shen B-G and Zhao J-G 1985 *Acta Phys. Sin.* **34** 1613
      (Also in *Landolt–Börnstein New Series* 1985 Group III, vol 19h (Berlin: Springer) p 188)
[16] Kemény T, Kaptás D, Balogh J, Kiss L F, Pusztai T and Vincze I 1999 *J. Phys.: Condens. Matter.* at press